agriculture

MDPI

Article

Estimating Winter Wheat Plant Nitrogen Content by Combining Spectral and Texture Features Based on a Low-Cost UAV RGB System throughout the Growing Season

Liyuan Zhang [1], Xiaoying Song [1], Yaxiao Niu [1,*], Huihui Zhang [2], Aichen Wang [1], Yaohui Zhu [1], Xingye Zhu [3], Liping Chen [1] and Qingzhen Zhu [4,*]

[1] School of Agricultural Engineering, Jiangsu University, Zhenjiang 212013, China
[2] Water Management and Systems Research Unit, USDA-ARS, 2150 Centre Avenue, Bldg. D., Fort Collins, CO 80526, USA
[3] Research Center of Fluid Machinery Engineering and Technology, Jiangsu University, Zhenjiang 212013, China
[4] High-Tech Key Laboratory of Agricultural Equipment and Intelligence of Jiangsu Province, Zhenjiang 212013, China
* Correspondence: yaxiao.niu@ujs.edu.cn (Y.N.); qingzhen_zhu@ujs.edu.cn (Q.Z.)

Abstract: As prior information for precise nitrogen fertilization management, plant nitrogen content (PNC), which is obtained timely and accurately through a low-cost method, is of great significance for national grain security and sustainable social development. In this study, the potential of the low-cost unmanned aerial vehicle (UAV) RGB system was investigated for the rapid and accurate estimation of winter wheat PNC across the growing season. Specifically, texture features were utilized as complements to the commonly used spectral information. Five machine learning regression algorithms, including support vector machines (SVMs), classification and regression trees, artificial neural networks, K-nearest neighbors, and random forests, were employed to establish the bridge between UAV RGB image-derived features and ground-truth PNC, with multivariate linear regression serving as the reference. The results show that both spectral and texture features had significant correlations with ground-truth PNC, indicating the potential of low-cost UAV RGB images to estimate winter wheat PNC. The H channel, S4O6, and R_SE and R_EN had the highest correlation among the spectral indices, Gabor texture features, and grey level co-occurrence matrix texture features, with absolute Pearson's correlation coefficient values of 0.63, 0.54, and 0.69, respectively. When the texture features were used together with spectral indices, the PNC estimation accuracy was enhanced, with the root mean square error (RMSE) decreasing from 2.56 to 2.24 g/kg, for instance, when using the SVM regression algorithm. The SVM regression algorithm with validation achieved the highest estimation accuracy, with a coefficient of determination (R^2) of 0.62 and an RMSE of 2.15 g/kg based on the optimal feature combination of B_CON, B_M, G_DIS, H, NGBDI, R_EN, R_M, R_SE, S3O7, and VEG. Overall, this study demonstrated that the low-cost UAV RGB system could be successfully used to map the PNC of winter wheat across the growing season.

Keywords: plant nitrogen content; UAV RGB images; gabor filter; grey level co-occurrence matrix; winter wheat

Citation: Zhang, L.; Song, X.; Niu, Y.; Zhang, H.; Wang, A.; Zhu, Y.; Zhu, X.; Chen, L.; Zhu, Q. Estimating Winter Wheat Plant Nitrogen Content by Combining Spectral and Texture Features Based on a Low-Cost UAV RGB System throughout the Growing Season. *Agriculture* **2024**, *14*, 456. https://doi.org/10.3390/agriculture14030456

Received: 12 February 2024
Revised: 5 March 2024
Accepted: 9 March 2024
Published: 11 March 2024

1. Introduction

Wheat is one of the three main cereal crops in China, and plays a critical role in national grain security and sustainable social development [1]. Nitrogen is one of the essential macronutrients required to maintain plant function and is a component of the chlorophyll molecule, which drives crop growth and grain production. Nitrogen deficiency could limit the photosynthesis of plants, resulting in a reduction in grain yield, whereas an overdose of nitrogen could lead to resource waste, soil acidification, and environmental pollution [2]. Therefore, precise nitrogen fertilization management, which requires the

estimation of plant nitrogen content (PNC) as prior information, is of great significance for national food security and sustainable development.

Traditionally, PNC was obtained using chemical analysis, in which crop plants need to be destructively sampled, dried to a constant weight (which usually takes days), weighed, and ground before the chemical analysis [3]. The disadvantages of the destructive, expensive, time-consuming, and laborious nature of the above method restricts its further application to large fields and the timely instruction of nitrogen fertilization management [4,5]. Obtaining the spatial–temporal information of PNC in a timely and accurate manner in large fields becomes one of the main limitations for precise nitrogen fertilization management.

With the development of remote sensing, various remote sensing platforms (satellites, unmanned aerial vehicles, near-ground, etc.) have been effective tools for the non-destructive acquisition of crop physiological and biochemical parameters [6–8]. Compared to satellite and ground-based remote sensing platforms, the unmanned aerial vehicle (UAV) remote sensing platform, with features including low cost, easy construction, high flexibility, and high spatial–temporal resolution, has become an advanced field information acquisition platform [9,10] and makes it possible to timely and accurately obtain high spatial–temporal PNC information in large fields [11].

In previous studies, when the UAV remote sensing platform was adopted to estimate the nitrogen information of crops, canopy spectral information was widely used based on the theory that the difference in crop nitrogen content leads to changes in crop morphological structure and leaf color; thus, the spectral information of these crops is also variable [12]. For example, the leaf nitrogen content of wheat was estimated based on canopy spectral information derived from UAV hyperspectral images [13] and UAV multispectral images [14]. However, although crop nitrogen content could be timely and accurately estimated in previous studies for wheat [13], maize [15], potato [16], rice [17], and citrus [18], it is still difficult for famers to accept the high price of UAV hyperspectral and multispectral systems in practical precise nitrogen fertilization management due to the relatively higher price of the hyperspectral and multispectral cameras. The potential of the UAV RGB system with a lower price should be explored for the rapid and accurate estimation of crop nitrogen content.

In addition, in previous studies, spectral information was always taken as input in estimation models of crop nitrogen content, which may perform poorly due to the impacts of soil information and high canopy biomass [19]. The above limitations of spectral information mean that crop nitrogen content could not be accurately obtained across the growing season due the periodic and drastic changes in soil information and crop biomass when spectral information was adopted separately. Texture information, which was usually used in image classification [20,21], is an essential complement to the spectral information and helps to segment objects or regions in an image. Similarly, the changes in crop morphological structure and leaf color, which are caused by crop nitrogen content differences, will also lead to changes in texture information [22,23], laying the theoretical basis for estimating crop nitrogen content using texture information. However, fewer studies have been conducted to estimate the PNC of winter wheat across the growing season based on both spectral information and texture features derived from UAV RGB images [24].

The main objectives of this study were as follows: (1) to evaluate the performance of the spectral and texture features derived from UAV RGB images in estimating the PNC of winter wheat; (2) to explore the optimal regression algorithm and input features for the accurate estimation of PNC; and (3) to timely and accurately obtain the winter wheat PNC distribution across the growing season, with high spatial–temporal resolution using the low-cost UAV RGB system.

2. Materials and Methods

2.1. Experiment Description

The research site was in Zhenjiang, Jiangsu province, China (31°57′48.9″ N, 119°17′54.5″ E, elevation 17 m), with the soil type classified as loamy sand according to the soil classification system developed by the United States Department of Agriculture [25]. The pH and organic matter content of the soil were 6.35 and 18.8 g/kg, respectively. The percentages of clay, powder, and sand in the soil layer were 1.27%, 10.42%, and 88.31%, respectively. Winter wheat, with five varieties of Yangmai29 (S1), Zhenmai15 (S2), Ningmaizi216 (S3), Yangmai25 (S4), and Zhenmai168 (S5), was planted on 10 Nov 2022 and was harvested on 7 Jun 2023. Five different nitrogen levels (i.e., 0 (N0), 90 (N1), 180 (N2), 270 (N3), and 360 (N4) kg/ha) were applied to the five winter wheat varieties, each with five replications. Namely, the experiment had a total of 25 treatments, comprising five nitrogen levels and five winter wheat species, each with five replications. This resulted in 125 experimental plots, each with an area of 4.8 m^2. Before the experiment began, soil samples were collected to test the content of total nitrogen, phosphorus, and potassium, with the results of 0.438, 0.460, and 13 g/kg, respectively. Figure 1 shows an overview of the experimental design in this study.

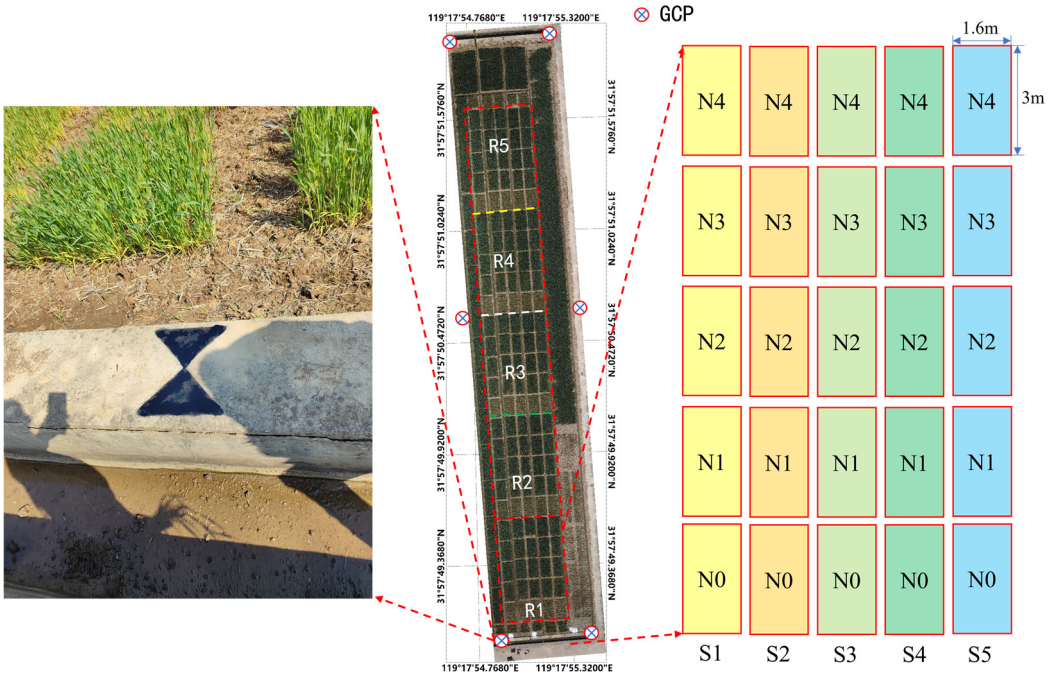

Figure 1. Overview of the winter wheat experimental design. R1–R5 presents replication areas of 1 to 5, N0–N4 represents nitrogen levels of 0 to 4, and S1–S5 represents winter wheat species of 1 to 5. GCP is the abbreviation used for ground control point.

2.2. Measurement of Plant Nitrogen Content of Winter Wheat

Samples of winter wheat plants in replications 1, 3, and 5 were destructively collected and placed in sealed bags from each plot at five key growth stages in 2023, including the jointing (08 April), flowering (20 April), filling (30 April), milk (8 May), and dough stages (23 May). After bringing these plant samples to the laboratory, they were oven-dried at 105 °C for 0.5 h and then at 80 °C for more than 48 h until the mass stabilized. After the dry mass was recorded, these dry samples were ground and their PNC values were determined using the Kjeldahl method [3]. Throughout the whole growing season, a total of 375 PNC samples were obtained. The outliers of PNC values were deleted for each growth stage, resulting in a total of 370 effective PNC samples.

2.3. UAV RGB Image Acquisition and Preprocessing

The UAV RGB images were collected on the same date using a Zenmuse P1 camera integrated on a DJI M300 RTK UAV platform (Da-Jiang Innovations, Shenzhen, China). The flight height, heading and side overlap, and ground sample distance were 30 m, 85% and 85%, and 3.7 mm, respectively. The Pix4DMapper software (Pix4D Inc., Prilly, Switzerland) was used to mosaic the UAV RGB images. The RTK differential GNSS device (CHCNAV, Shanghai, China) was utilized to measure the coordinates of the ground control points shown in Figure 1 and to correct the geographic location information of the images. The shapefile data of 125 plots (Figure 1), which were manually derived using ENVI 5.3 software (Harris Corp, Bloomfield, CO, USA), were used to extract the regions of interest from the ortho-mosaic using R language.

2.4. Calculation of Spectral Indices and Texture Features

The three single-bands (red, blue, and green), H channel derived from the HSV color space, A channel derived from the Lab color space, and eight vegetation indices (hereafter noted as spectral indices) were selected as the inputs for the regression model to estimate the PNC of winter wheat. Table 1 shows the calculation formulas of the eight vegetation indices. Except for the above spectral indices, the texture features, derived using both the Gabor [26] and the grey level co-occurrence matrix (GLCM) [23] methods, were also adopted as inputs to estimate the PNC. Specifically, the Gabor textures were calculated from RGB images with Gabor filters of size 5×5 obtained at 5 scales and 8 orientations. A total of 40 Gabor texture features were constructed and noted using the number of scale and orientation. For example, the Gabor texture feature of S1O2 means that it was obtained under the first scale and the second orientation. The contrast (CON), entropy (EN), variance (VAR), mean (M), homogeneity (HOM), dissimilarity (DIS), and second moment (SE) were selected as GLCM texture features and were derived from red, blue, and green bands using the smallest window size (3×3 pixels). Therefore, a total of 21 GLCM texture features were chosen. Finally, a total of 13 spectral indices, 40 Gabor texture features, and 21 GLCM texture features were selected to estimate the PNC of winter wheat across the growing season.

Table 1. Vegetation indices used in this study. R, G, and B are the abbreviations for the red, green, and blue bands.

Vegetation Index	Formula
Visible atmospherically resistant index [27]	$VARI = (G - R)/(G + R - B)$
Vegetative index [28]	$VEG = G/(R^{0.667} * B^{(1-0.667)})$
Green–red vegetation index [29]	$GRVI = (G - R)/(G + R)$
Excess green index [30]	$ExG = 2G - R - B$
Excess G minus excess red index [31]	$ExGR = 3G - 2.4R - B$
Red–green ratio index [32]	$RGRI = R/G$
Normalized blue–red difference index [27]	$NGRDI = (G - R)/(G + R)$
Normalized blue–green difference index [33]	$NGBDI = (G - B)/(G + B)$

2.5. Machine Learning Modelling and Statistical Analysis

To establish the PNC regression model based on the features derived from the UVA RGB images and to evaluate their applicability, the whole dataset was divided into two parts, namely the training dataset, with data pairs collected in replications 1 and 5, and the validation dataset, with data pairs collected in replication 3. Table 2 shows the basic statistics of the PNC of winter wheat at different growth stages for the two datasets.

Table 2. Basic statistics of the plant nitrogen content (PNC) of winter wheat at different growth stages for the two datasets.

Dataset	Stage	Min (g/kg)	Max (g/kg)	Mean (g/kg)	CV (%)
Training	Jointing	6.86	27.00	15.01	35.49
	Flowering	5.16	12.96	8.71	26.13
	Filling	4.33	13.63	8.02	28.44
	Milk	4.09	11.20	7.49	25.55
	Dough	2.53	10.78	7.26	26.08
Validation	Jointing	6.63	23.55	13.28	35.39
	Flowering	4.89	12.00	8.01	27.25
	Filling	4.28	11.56	7.93	25.42
	Milk	4.12	11.47	7.86	27.53
	Dough	4.46	9.81	6.70	23.31

Five machine learning regression algorithms, including the K-nearest neighbor (KNN), classification and regression tree (CART), artificial neural network (ANN), support vector machines (SVMs), and random forest (RF) regression algorithms, were chosen to establish the PNC estimation models, using the multivariate linear regression (MLR) algorithm as the reference. The CART, KNN, ANN, SVM, RF, and MLR algorithms were implemented using the "rpart", "kknn", "nnet", "e1071", "randomForest", and "lm" packages in the R language. The coefficient of determination (R^2) and the root mean square error (RMSE) were calculated for the evaluation.

To reduce the redundancy of each input dataset and decrease the computational burden, the mRMR method [34] was used first to select the top 8 scored features for spectral indices, Gabor texture features, and GLCM texture features, respectively. Then, the Wrapper method [35], with a sequential forward fashion, was adopted to further filter the optimal combination of SI and texture features for each regression algorithm, using RMSE as the evaluation indicator. A total of seven feature combinations were used in this study, including spectral indices (SIs), Gabor texture features (Gabor), GLCM texture features (GLCMs), SI plus Gabor, SI plus GLCM, Gabor plus GLCM, and SI plus Gabor and GLCM.

3. Results

3.1. Variation in the PNC of Winter Wheat across the Growing Season

To confirm that different nitrogen levels were successfully applied across the growing season, bar plots of PNC were drawn for the five key growth stages of winter wheat, with nitrogen application levels and winter wheat species as the two factors. As shown in Figure 2, with an increase in nitrogen application levels, an increasing trend of PNC was observed in most of the growth stages for most of the five species. Taking the PNC values of species 1, for example, in the flowering stage, the mean PNC values for the five nitrogen application levels were 6.00, 6.96, 8.68, 9.31, and 10.26 g/kg, respectively. At the same time, it was observed that the relationship of the PNC values of N2, N3, and N4, which were greater, was not stable. As for species 2, in the flowering stage, the PNC values for N2, N3, and N4 were 9.96, 10.18, and 10.48, respectively. In the milk stage of species 2, the PNC values for N2, N3, and N4 were 8.60, 9.38, and 8.41, respectively. When observing the PNC trend across the growing season, similar trends were observed for the five winter wheat species; that is, they gradually decreased from the jointing stage to the dough stage, with mean PNC values of 14.43, 8.24, 8.04, 7.72, and 7.13 g/kg for species 1, for example. Overall, different nitrogen stress statuses were successfully applied for five winter wheat species across the growing season.

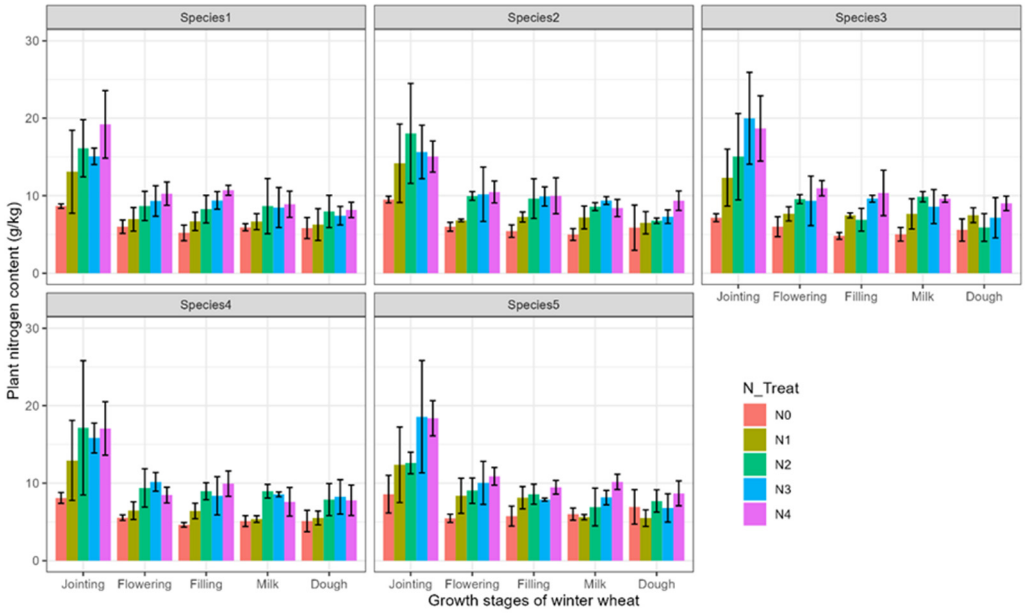

Figure 2. Plant nitrogen content (PNC) bar plots, which were drawn for the five key growth stages of winter wheat, with nitrogen application levels and winter wheat species as two factors.

3.2. Correlation between PNC and Each Individual Feature Derived from UAV RGB Images

As shown in Figure 3, H, RGRI, B, VEG, VARI, NGBDI, G, and GRVI were selected using the mRMR method for spectral indices. S2O1, S2O5, S2O8, S3O3, S3O4, S3O7, S4O4, and S4O6 were selected as the Gabor texture features. As for the GLCM texture features, they were R_SE, R_M, B_CON, B_M, B_SE, G_VAR, G_DIS, and R_EN. Specifically, among the eight spectral indices, the H channel had the highest positive correlation with PNC, with a Pearson's correlation coefficient (r) value of 0.63, and GRVI had the lowest negative correlation, with an r value of −0.32. When it comes to the Gabor texture features, S4O6 had the highest negative correlation, with an r value of −0.53, and S_2O_8 had the lowest positive correlation, with an r value of 0.16. As for the GLCM texture features, a higher correlation was found, with a highest absolute r value of 0.69 for both R_EN and R_SE. The lowest negative correlation was observed for B_CON, with an r value of −0.22. Overall, significant correlations with PNC were found for the spectral indices and the texture features, which were derived from UAV RGB images, indicating that they could be used as inputs for the PNC regression models.

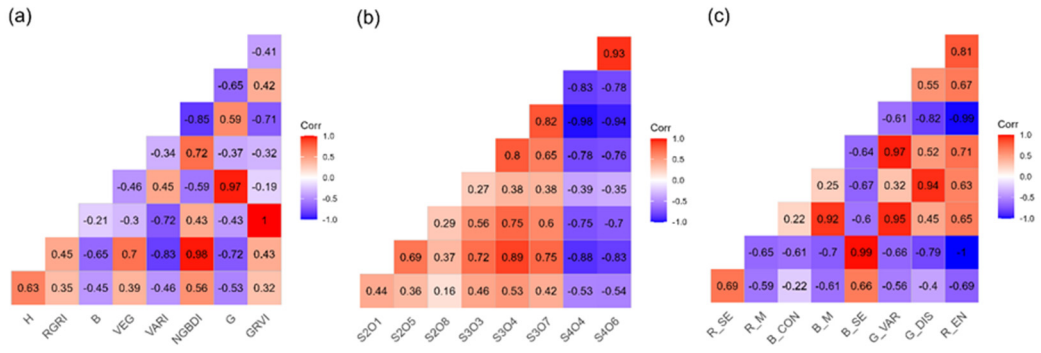

Figure 3. Pearson's correlation coefficient (r) between PNC and each individual feature derived from the UAV RGB images. (**a**) Spectral indices, (**b**) Gabor texture features, and (**c**) GLCM texture features.

3.3. Extraction of Optimal Features Derived from UAV RGB Images

Figure 4 shows the PNC estimation accuracy derived from the six regression algorithms based on the optimal feature combination for each of the seven feature categories.

Among the seven feature categories, the Gabor category had the lowest PNC estimation performance for all of the six algorithms, with an RMSE that ranged from 3.17 to 3.50 g/kg. The GLCM texture feature category had the best performance when one of the SI, Gabor, or GLCM categories was individually adopted. The RMSE for CART, KNN, ANN, SVM, RF, and MLR was 2.50, 2.45, 2.29, 2.36, 2.32, and 2.59 g/kg, respectively. Only the RMSE of MLR was higher than for the SI feature category (2.54 g/kg). When the SI and GLCM features were taken as inputs for the PNC regression models together, the performance of CART, KNN, and MLR were improved, with an RMSE that decreased from 2.50 to 2.35 g/kg, from 2.45 to 2.32 g/kg, and from 2.59 to 2.31 g/kg, respectively. The PNC estimation performance of KNN, SVM, and RF was further improved when the Gabor features were adopted together with the SI and GLCM features, with an RMSE that decreased from 2.32 to 2.25 g/kg, 2.30 to 2.24 g/kg, and 2.33 to 2.25 g/kg, respectively. As for the performance of CART and MLR, they remained relatively stable, with an RMSE of 2.31 and 2.32 g/kg, respectively. Overall, the combination of SI, Gabor, and GLCM features exhibited the best PNC estimation performance for each of the six regression algorithms. Table 3 shows the optimal features for each regression algorithm.

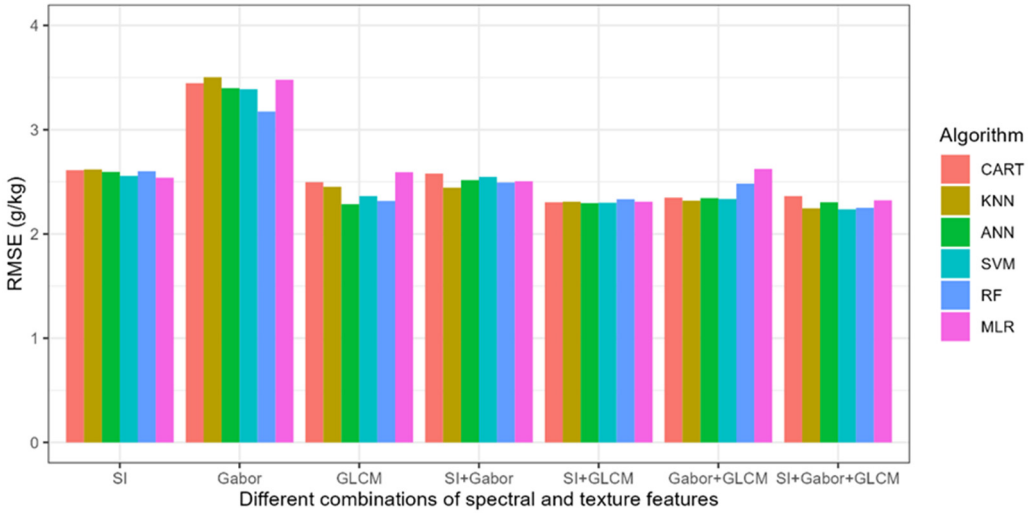

Figure 4. PNC estimation accuracy derived from the six regression algorithms based on the optimal feature combination for each of the seven feature categories.

Table 3. The optimal features for each PNC regression algorithm when the spectral indices, Gabor, and GLCM texture features were all taken into consideration.

Category	Algorithm	Optimal Features
SI + Gabor + GLCM	CART	G_DIS, NGBDI, R_EN, R_M, S3O4
SI + Gabor + GLCM	KNN	B_SE, G_VAR, H, R_EN, R_SE, S4O4
SI + Gabor + GLCM	ANN	B_CON, NGBDI, R_SE, S3O7
SI + Gabor + GLCM	SVM	B_CON, B_M, G_DIS, H, NGBDI, R_EN, R_M, R_SE, S3O7, VEG
SI + Gabor + GLCM	RF	B_CON, B_SE, NGBDI, S2O8, S3O4
SI + Gabor + GLCM	MLR	B, B_CON, B_SE, G, G_DIS, H, NGBDI, R_EN, R_M, R_SE, S2O8, S3O4, S4O4, VEG

3.4. Evaluation of PNC Estimation Models Established Based on the Optimal Features

Figure 5 shows the correlation between the estimated PNC and the ground-truth PNC. When the data collected in replication 3 were used for the evaluation, all PNC models, which were established from the six regression algorithms based on their corresponding optimal features, could be successfully used to estimate the PNC of winter wheat, with an R^2 that ranged from 0.38 to 0.62 and an RMSE that ranged from 2.76 to 2.15 g/kg. Among the six regression algorithms, the PNC estimation model established from the SVM exhibited the best performance, with an R^2 of 0.62 and an RMSE of 2.15 g/kg, followed

by MLR, with an R^2 of 0.59 and an RMSE of 2.23 g/kg. The performance of the other four machine learning algorithms (CART, KNN, ANN, and RF) were all lower than MLR, with an R^2 that ranged from 0.38 to 0.54 and an RMSE that ranged from 2.76 to 2.37 g/kg. In addition, a more dispersed distribution was observed for the jointing stage compared to the other four key growth stages of winter wheat. Overall, the PNC estimation model established from the SVM regression algorithm based on the optimal features of B_CON, B_M, G_DIS, H, NGBDI, R_EN, R_M, R_SE, S3O7, and VEG exhibited the best performance. Therefore, the SVM model was chosen to map the PNC of winter wheat.

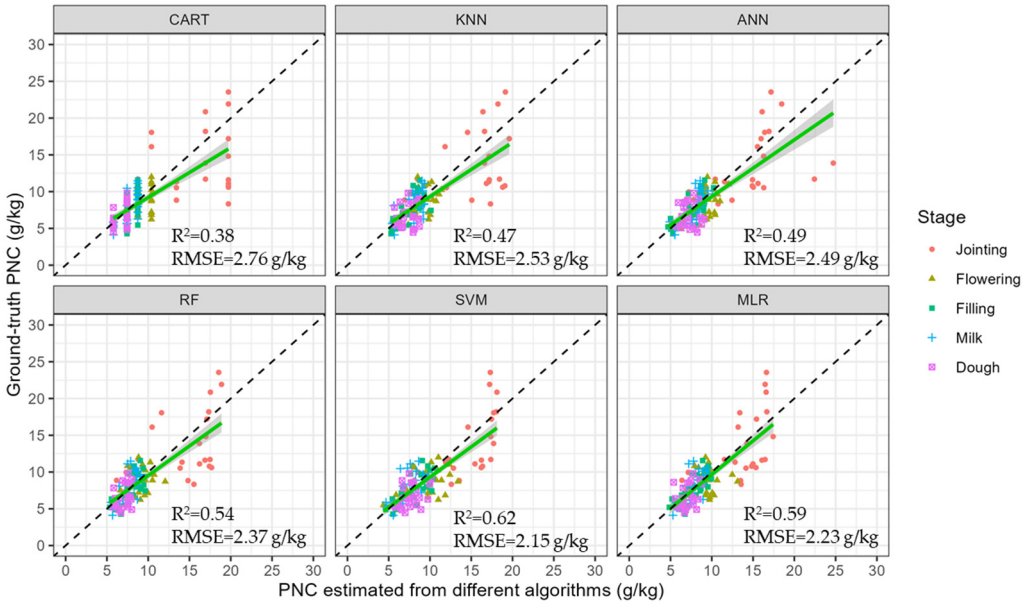

Figure 5. Estimation performance of the PNC models, which were established based on corresponding optimal features. The black dashed line is 1:1 line.

3.5. Mapping PNC Using the SVM Regression Model Based on UAV RGB Images

As shown in Figure 6, a similar trend of winter wheat PNC, as depicted in Figure 2, was found among different nitrogen application levels. Namely, an increasing trend of PNC was observed with increasing nitrogen application. PNC differences among the different winter wheat species were also found. In the dough stage, this phenomenon was more obvious. Different ripeness was observed on 23 May 2023 (dough stage), resulting in a relatively greener plant with a higher PNC. In addition, due to field heterogeneity, PNC differences were also observed in each small plot, demonstrating the significance of capturing the spatial–temporal distribution of PNC.

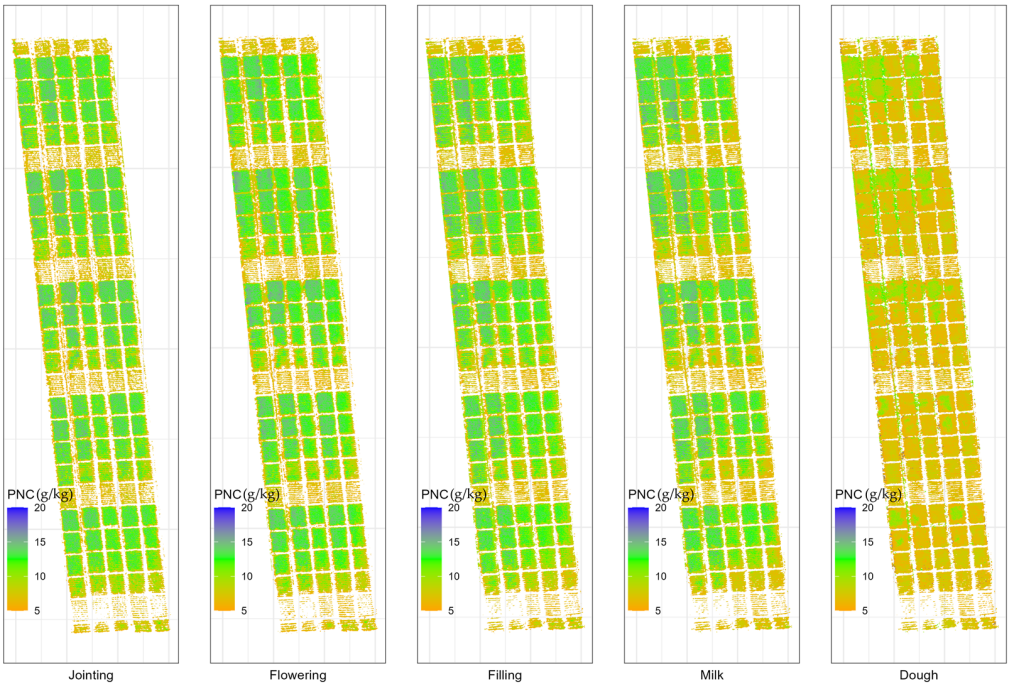

Figure 6. PNC maps of winter wheat obtained from the UAV RGB images and the SVM regression algorithm.

4. Discussion

PNC, which is an important indicator of nutritional status, could be used to generate nitrogen fertilizer prescriptions to guide precise nitrogen fertilization management [36]. The timely and accurate acquisition of the high spatial–temporal distribution of PNC through a low-cost method will accelerate the process for famers using PNC information to guide precise nitrogen fertilization management. Different to previous studies, the UAV hyperspectral or multispectral system was replaced by a low-cost UAV RGB system in this study to map the PNC of winter wheat across the growing season. Spectral and texture features derived from UAV RGB images were used as inputs for machine learning regression algorithms to estimate PNC.

Similar to the spectral information derived from UAV hyperspectral or multispectral images [14,15], a significant correlation was found between the spectral index derived from UAV RGB images and the ground-truth PNC. The highest correlation, with a positive r value of 0.63, was found for the H channel of the HSV color space, which was higher than the green band, which had a negative r value of −0.53. The reason may be that, compared to the RGB space, H represents the hue, which refers to pure color [37], making it more sensitive to capturing the color changes caused by nitrogen nutrition differences. As is well known, nitrogen deficiency can lead to decreased crop chlorophyll content, which subsequently leads to leaf yellowing [38]. A significant correlation between the UAV RGB spectral index and the ground-truth PNC or leaf nitrogen content has also been observed for cotton [39], potato [40], sugarcane [41], and winter wheat [42,43].

When using UAV RGB images to estimate the plant or leaf nitrogen content of winter wheat, two main drawbacks were identified in previous studies [24,42,43]. Firstly, reliance solely on spectral features (usually the vegetation indices). Secondly, the absence of a universal nitrogen content estimation model across the growing season. The main drawback of spectral information in estimating crop growth information is that its performance could be affected by soil information and high canopy biomass [19]. In addition to spectral information, the potential of UAV RGB images should be further explored for the accurate estimation of PNC across the growing season for winter wheat. In this study, texture features derived from UAV RGB images were used as a complement to spectral information to establish a universal estimation model of winter wheat PNC across the growing season.

Specifically, both Gabor and GLCM texture features had significant correlations with the ground-truth PNC. The highest negative r value of −0.54 was observed for the S4O6 Gabor texture feature, and the GLCM texture features of R_SE and R_EN had the highest correlation, with an absolute r value of 0.69. When it comes to estimating PNC across the growing season, higher estimation performance was achieved by the combining spectral indices and texture features (Figures 4 and 5). The SVM regression algorithm exhibited the best performance, with a validation R^2 of 0.62 and an RMSE of 2.15 g/kg based on the optimal feature combination of B_CON, B_M, G_DIS, H, NGBDI, R_EN, R_M, R_SE, S3O7, and VEG. Compared to UAV multispectral images, comparable crop nitrogen content estimation performance was achieved. For example, the leaf nitrogen content estimation model of wheat was established based on the NDVI (730, 850) across the growing season, with a validation R^2 of 0.6037 and a relative RMSE of 0.1217 [23]. Overall, in this study, the UAV RGB system proved to be an effective low-cost tool for mapping winter wheat PNC across the whole growing season.

5. Conclusions

The results show that both spectral and texture features derived from low-cost UAV RGB images had a significant correlation with the ground-truth PNC of winter wheat. The H channel of the HSV color space among the eight spectral indices exhibited the highest correlation, with a positive r value of 0.63, which was higher than the green band, with a negative r value of −0.53. The reason for this may be that the H channel, which refers to pure color, is more sensitive to the color changes caused by nitrogen nutrition deficiency. Among the eight Gabor texture features, S4O6 had the highest negative correlation, with an r value of −0.54. The GLCM texture features of R_SE and R_EN had the highest correlation, with an absolute r value of 0.69. When the texture features were taken as a complement to spectral indices, the PNC estimation performance was enhanced across the growing season. The highest estimation accuracy was achieved using the SVM regression algorithm, with a validation R^2 of 0.62 and an RMSE of 2.15 g/kg based on the optimal feature combination of B_CON, B_M, G_DIS, H, NGBDI, R_EN, R_M, R_SE, S3O7, and VEG. Overall, this study demonstrated that the low-cost UAV RGB system could be successfully used to map the PNC of winter wheat across the growing season.

Author Contributions: Conceptualization, visualization, and writing—original draft preparation, L.Z. and Y.N.; data curation, methodology, and software, X.S., Y.Z. and X.Z.; validation and formal analysis, A.W. and H.Z.; investigation, resources, conceptualization, writing—review and editing, and funding acquisition, Q.Z. and L.C. All authors have read and agreed to the published version of the manuscript.

Funding: This research was funded by the National Natural Science Foundation of China (No. 52309051, 32001417), the Natural Science Foundation of Jiangsu Province (No. BK20230548), the China Postdoctoral Science Foundation (No. 2022T150276), and the Key R&D Project of Jiangsu Province (Modern Agriculture, BE2022351).

Institutional Review Board Statement: Not applicable.

Data Availability Statement: The original contributions presented in this study are included in the article. Further inquiries can be directed to the corresponding authors.

Acknowledgments: The authors wish to thank all those who helped with this research.

Conflicts of Interest: The authors declare no conflicts of interest.

Nomenclature

PNC	Plant nitrogen content	UAV	Unmanned aerial vehicle
H channel	Hue in Hue–Saturation–Intensity color space	SiOj	Gabor feature derived at a scale of i and orientations of j
GLCM	Grey level co-occurrence matrix	VARI	Visible atmospherically resistant index
CON	Contrast in GLCM	VEG	Vegetative index
EN	Entropy in GLCM	GRVI	Green–red vegetation index
VAR	Variance in GLCM	ExG	Excess green index
M	Mean in GLCM	ExGR	Excess G minus excess red index
HOM	Homogeneity in GLCM	RGRI	Red–green ratio index
DIS	Dissimilarity in GLCM	NGRDI	Normalized blue–red difference index
SE	Second moment in GLCM	NGBDI	Normalized blue–green difference
R	Red	KNN	K-nearest neighbor
G	Blue	CART	Classification and regression tree
B	Green	ANN	Artificial neural network
R/G/B_ CON	CON from red/green/blue	SVM	Support vector machine
R/G/B_ DIS	DIS from red/green/blue	RF	Random forest
R/G/B_ EN	EN from red/green/blue	MLR	Multivariate linear regression
R/G/B_ M	M from red/green/blue	RMSE	Root mean square error
R/G/B_ SE	SE from red/green/blue	R^2	Coefficient of determination
R/G/B_ VAR	VAR from red/green/blue	CV	Convariance
SI	Spectral indices		

References

1. Yin, Q.; Zhang, Y.; Li, W.; Wang, J.; Wang, W.; Ahmad, I.; Zhou, G.; Huo, Z. Estimation of Winter Wheat SPAD Values Based on UAV Multispectral Remote Sensing. *Remote Sens.* **2023**, *15*, 3595. [CrossRef]
2. Li, X.; Hu, C.; Delgado, J.A.; Zhang, Y.; Ouyang, Z. Increased nitrogen use efficiencies as a key mitigation alternative to reduce nitrate leaching in north china plain. *Agric. Water Manag.* **2007**, *89*, 137–147. [CrossRef]
3. Sáez-Plaza, P.; Navas, M.J.; Wybraniec, S.; Michałowski, T.; Asuero, A.G. An overview of the Kjeldahl method of nitrogen determination. Part II. Sample preparation, working scale, instrumental finish, and quality control. *Crit. Rev. Anal. Chem.* **2013**, *43*, 224–272. [CrossRef]
4. Verma, B.; Prasad, R.; Srivastava, P.K.; Singh, P.; Badola, A.; Sharma, J. Evaluation of Simulated AVIRIS-NG Imagery Using a Spectral Reconstruction Method for the Retrieval of Leaf Chlorophyll Content. *Remote Sens.* **2022**, *14*, 3560. [CrossRef]
5. Argento, F.; Anken, T.; Abt, F.; Vogelsanger, E.; Walter, A.; Liebisch, F. Site-specific nitrogen management in winter wheat supported by low-altitude remote sensing and soil data. *Precis. Agric.* **2021**, *22*, 364–386. [CrossRef]
6. Zhen-qi, L.; Yu-long, D.; Han, W.; Ketterings, Q.M.; Jun-sheng, L.; Fu-cang, Z.; Zhi-jun, L.; Jun-liang, F. A double-layer model for improving the estimation of wheat canopy nitrogen content from unmanned aerial vehicle multispectral imagery. *J. Integr. Agric.* **2023**, *22*, 2248–2270. [CrossRef]
7. Pereira, F.R.d.S.; de Lima, J.P.; Freitas, R.G.; Dos Reis, A.A.; Amaral, L.R.d.; Figueiredo, G.K.D.A.; Lamparelli, R.A.C.; Magalhães, P.S.G. Nitrogen variability assessment of pasture fields under an integrated crop-livestock system using UAV, PlanetScope, and Sentinel-2 data. *Comput. Electron. Agric.* **2022**, *193*, 106645. [CrossRef]
8. Zhang, L.; Zhang, H.; Han, W.; Niu, Y.; Chávez, J.L.; Ma, W. The mean value of gaussian distribution of excess green index: A new crop water stress indicator. *Agric. Water Manag.* **2021**, *251*, 106866. [CrossRef]
9. Zhang, L.; Niu, Y.; Zhang, H.; Han, W.; Li, G.; Tang, J.; Peng, X. Maize Canopy Temperature Extracted From UAV Thermal and RGB Imagery and Its Application in Water Stress Monitoring. *Front. Plant Sci.* **2019**, *10*, 1270. [CrossRef]
10. Zhang, L.; Zhang, H.; Niu, Y.; Han, W. Mapping maize water stress based on UAV multispectral remote sensing. *Remote Sens.* **2019**, *11*, 605. [CrossRef]
11. Wang, S.-M.; Ma, J.-H.; Zhao, Z.-M.; Yang, H.-Z.-Y.; Xuan, Y.-M.; Ouyang, J.-X.; Fan, D.-M.; Yu, J.-F.; Wang, X.-C. Pixel-class prediction for nitrogen content of tea plants based on unmanned aerial vehicle images using machine learning and deep learning. *Expert Syst. Appl.* **2023**, *227*, 120351. [CrossRef]

12. Haboudane, D.; Miller, J.R.; Tremblay, N.; Zarco-Tejada, P.J.; Dextraze, L. Integrated narrow-band vegetation indices for prediction of crop chlorophyll content for application to precision agriculture. *Remote Sens. Environ.* **2002**, *81*, 416–426. [CrossRef]
13. Ma, X.; Chen, P.; Jin, X. Predicting Wheat Leaf Nitrogen Content by Combining Deep Multitask Learning and a Mechanistic Model Using UAV Hyperspectral Images. *Remote Sens.* **2022**, *14*, 6334. [CrossRef]
14. Pan, Y.; Wu, W.; Zhang, J.; Zhao, Y.; Zhang, J.; Gu, Y.; Yao, X.; Cheng, T.; Zhu, Y.; Cao, W.; et al. Estimating leaf nitrogen and chlorophyll content in wheat by correcting canopy structure effect through multi-angular remote sensing. *Comput. Electron. Agric.* **2023**, *208*, 107769. [CrossRef]
15. Jia, Z.; Zhao, S.; Zhang, Q.; Xia, C.; Zhang, X.; Zhang, Y.; Gao, Q. Multi-stage fertilizer recommendation for spring maize at the field scale based on narrowband vegetation indices. *Comput. Electron. Agric.* **2023**, *213*, 108236. [CrossRef]
16. Fan, Y.; Feng, H.; Yue, J.; Liu, Y.; Jin, X.; Xu, X.; Song, X.; Ma, Y.; Yang, G. Comparison of Different Dimensional Spectral Indices for Estimating Nitrogen Content of Potato Plants over Multiple Growth Periods. *Remote Sens.* **2023**, *15*, 602. [CrossRef]
17. Liang, T.; Duan, B.; Luo, X.; Ma, Y.; Yuan, Z.; Zhu, R.; Peng, Y.; Gong, Y.; Fang, S.; Wu, X. Identification of High Nitrogen Use Efficiency Phenotype in Rice (*Oryza sativa* L.) Through Entire Growth Duration by Unmanned Aerial Vehicle Multispectral Imagery. *Front. Plant Sci.* **2021**, *12*, 740414. [CrossRef]
18. Termin, D.; Linker, R.; Baram, S.; Raveh, E.; Ohana-Levi, N.; Paz-Kagan, T. Dynamic delineation of management zones for site-specific nitrogen fertilization in a citrus orchard. *Precis. Agric.* **2023**, *24*, 1570–1592. [CrossRef]
19. Zhang, J.; Liu, X.; Liang, Y.; Cao, Q.; Tian, Y.; Zhu, Y.; Cao, W.; Liu, X. Using a Portable Active Sensor to Monitor Growth Parameters and Predict Grain Yield of Winter Wheat. *Sensors* **2019**, *19*, 1108. [CrossRef]
20. Laliberte, A.S.; Rango, A. Texture and scale in object-based analysis of subdecimeter resolution unmanned aerial vehicle (UAV) imagery. *IEEE Trans. Geosci. Remote Sens.* **2009**, *47*, 761–770. [CrossRef]
21. Murray, H.; Lucieer, A.; Williams, R. Texture-based classification of sub-Antarctic vegetation communities on Heard Island. *Int. J. Appl. Earth Obs. Geoinf.* **2010**, *12*, 138–149. [CrossRef]
22. Zhang, J.; Qiu, X.; Wu, Y.; Zhu, Y.; Cao, Q.; Liu, X.; Cao, W. Combining texture, color, and vegetation indices from fixed-wing UAS imagery to estimate wheat growth parameters using multivariate regression methods. *Comput. Electron. Agric.* **2021**, *185*, 106138. [CrossRef]
23. Fu, Z.; Yu, S.; Zhang, J.; Xi, H.; Gao, Y.; Lu, R.; Zheng, H.; Zhu, Y.; Cao, W.; Liu, X. Combining UAV multispectral imagery and ecological factors to estimate leaf nitrogen and grain protein content of wheat. *Eur. J. Agron.* **2022**, *132*, 126405. [CrossRef]
24. Yang, B.; Wang, M.; Sha, Z.; Wang, B.; Chen, J.; Yao, X.; Cheng, T.; Cao, W.; Zhu, Y. Evaluation of Aboveground Nitrogen Content of Winter Wheat Using Digital Imagery of Unmanned Aerial Vehicles. *Sensors* **2019**, *19*, 4416. [CrossRef] [PubMed]
25. Soil Survey Staff, S.T. *A Basic System of Soil Classification for Making and Interpreting Soil Surveys*; US Department of Agriculture, Natural Resources Conservation Service, National Soil Survey Center: Lincoln, NE, USA, 1999.
26. Granlund, G.H. In search of a general picture processing operator. *Comput. Graph. Image Process.* **1978**, *8*, 155–173. [CrossRef]
27. Gitelson, A.A.; Kaufman, Y.J.; Stark, R.; Rundquist, D. Novel algorithms for remote estimation of vegetation fraction. *Remote Sens. Environ.* **2002**, *80*, 76–87. [CrossRef]
28. Hague, T.; Tillett, N.D.; Wheeler, H. Automated crop and weed monitoring in widely spaced cereals. *Precis. Agric.* **2006**, *7*, 21–32. [CrossRef]
29. Tucker, C.J. Red and photographic infrared linear combinations for monitoring vegetation. *Remote Sens. Environ.* **1979**, *8*, 127–150. [CrossRef]
30. Woebbecke, D.M.; Meyer, G.E.; Von Bargen, K.; Mortensen, D.A. Color indices for weed identification under various soil, residue, and lighting conditions. *Trans. ASAE* **1995**, *38*, 259–269. [CrossRef]
31. Meyer, G.E.; Neto, J.C. Verification of color vegetation indices for automated crop imaging applications. *Comput. Electron. Agric.* **2008**, *63*, 282–293. [CrossRef]
32. Gamon, J.A.; Surfus, J.S. Assessing leaf pigment content and activity with a reflectometer. *New Phytol.* **1999**, *143*, 105–117. [CrossRef]
33. Hunt, E.R.; Cavigelli, M.; Daughtry, C.S.T.; McMurtrey, J.E.; Walthall, C.L. Evaluation of digital photography from model aircraft for remote sensing of crop biomass and nitrogen status. *Precis. Agric.* **2005**, *6*, 359–378. [CrossRef]
34. Ding, C.; Peng, H. Minimum redundancy feature selection from microarray gene expression data. *J. Bioinform Comput. Biol.* **2005**, *3*, 185–205. [CrossRef] [PubMed]
35. Kohavi, R.; John, G.H. Wrappers for feature subset selection. *Artif. Intell.* **1997**, *97*, 273–324. [CrossRef]
36. Yang, M.; Xu, X.; Li, Z.; Meng, Y.; Yang, X.; Song, X.; Yang, G.; Xu, S.; Zhu, Q.; Xue, H. Remote Sensing Prescription for Rice Nitrogen Fertilizer Recommendation Based on Improved NFOA Model. *Agronomy* **2022**, *12*, 1804. [CrossRef]
37. Joblove, G.H.; Greenberg, D. Color spaces for computer graphics. *ACM SIGGRAPH COMPUT. GRAPH.* **1978**, *12*, 20–25. [CrossRef]
38. Wei, Q.; Zhang, B.Z.; Wei, Z.; Han, X.; Duan, C.F. Estimation of canopy chlorophyll content in winter wheat by UAV multispectral remote sensing. *J. Triticeae Crops* **2020**, *40*, 365–372.
39. Kou, J.; Duan, L.; Yin, C.; Ma, L.; Chen, X.; Gao, P.; Lv, X. Predicting Leaf Nitrogen Content in Cotton with UAV RGB Images. *Sustainability* **2022**, *14*, 9259. [CrossRef]
40. Fan, Y.-G.; Feng, H.-K.; Liu, Y.; Bian, M.-B.; Zhao, Y.; Yang, G.-J.; Qian, J.-G. Estimation of Nitrogen Content in Potato Plants Based on Spectral Spatial Characteristics. *Spectrosc. Spectr. Anal.* **2023**, *43*, 1532–1540.

41. Hosseini, S.A.; Masoudi, H.; Sajadiye, S.M.; Mehdizadeh, S.A. Nitrogen Estimation in Sugarcane Fields from Aerial Digital Images Using Artificial Neural Network. *Environ. Eng. Manag. J.* **2021**, *20*, 713–723.
42. Song, X.; Yang, G.; Xu, X.; Zhang, D.; Yang, C.; Feng, H. Winter Wheat Nitrogen Estimation Based on Ground-Level and UAV-Mounted Sensors. *Sensors* **2022**, *22*, 549. [CrossRef] [PubMed]
43. Jiang, J.; Cai, W.; Zheng, H.; Cheng, T.; Tian, Y.; Zhu, Y.; Ehsani, R.; Hu, Y.; Niu, Q.; Gui, L.; et al. Using Digital Cameras on an Unmanned Aerial Vehicle to Derive Optimum Color Vegetation Indices for Leaf Nitrogen Concentration Monitoring in Winter Wheat. *Remote Sens.* **2019**, *11*, 2667. [CrossRef]